A bio-inspired, active morphing skin for camber morphing structures

2015 Smart Mater. Struct. 24 035023

(http://iopscience.iop.org/0964-1726/24/3/035023)

IOP Publishing Smart Materials and Structures
Smart Mater. Struct. **24** (2015) 035023 (7pp) doi:10.1088/0964-1726/24/3/035023

A bio-inspired, active morphing skin for camber morphing structures

Ning Feng[1], Liwu Liu[2], Yanju Liu[2] and Jinson Leng[1]

[1] Centre for Composite Materials, Science Park of Harbin Institute of Technology (HIT), PO Box 3011, No. 2 YiKuang Street, Harbin 150080, People's Republic of China
[2] Department of Astronautical Science and Mechanics, Harbin Institute of Technology (HIT), PO Box 301, No. 92 West Dazhi Street, Harbin 150001, People's Republic of China

E-mail: lengjs@hit.edu.cn

Received 10 November 2014
Accepted for publication 12 January 2015
Published 13 February 2015

Abstract

In this study, one kind of developed morphing skin embedded with pneumatic muscle fibers (PMFs) was manufactured and was employed for camber morphing structures. The output force and contraction of PMF as well as the morphing skin were experimentally characterized at a series of discrete actuator pressures varying from 0.15 to 0.35 MPa. The active morphing skin test results show that the output force is 73.59 N and the contraction is 0.097 (9.7%) at 0.35 MPa. Due to these properties, this active morphing skin could be easily used for the morphing structures. Then the proper airfoil profile was chosen to manufacture the adaptive airfoil in this study. The chord-wise bending airfoil structure was achieved by employing this kind of active morphing skin. Finally the deformed shapes of this chord-wise bending airfoil structure were obtained by 3-dimensions scanning measurement. Meanwhile the camber morphing structures were analyzed through the finite element method (FEM) and the deformed shapes of the upper surface skins were obtained. The experimental result and FEM analysis result of deformed shapes of the upper surface skins were compared in this paper.

Keywords: pneumatic muscle fiber, active morphing skin, camber morphing structure, chord-wise bending airfoil, finite element analysis

(Some figures may appear in colour only in the online journal)

1. Introduction

For thousands of years, humans have been dreamed of flying like a bird. Although Wright brothers designed and manufactured the first aircraft with the flexible wing which could be easily warped using cables and pulleys as a way to provide stability and control [1, 2], it was not the morphing aircraft of the real meaning. For over one century, most of aircrafts have possessed rigid structures to execute the single mission, such as high maneuverability, long loiter, or extreme speeds [3]. In view of this, morphing aircrafts with flexible frames as one kind of multiple mission vehicles tend to be compromises of the different missions. The optimal objective can be realized by changing the aerodynamic layout of morphing aircraft according to the flight mission [3]. Sofla *et al* [4] classified the wing morphing concepts into three major types: plan form alternation, out-of-plane transformation, and airfoil adjustment. Sofla *et al* [5] developed a series of SMA-actuated flexural structures which could be used to deform wing sections. In these flexural sections chord-wise bending could be achieved by the heating of SMA strips in an antagonistic design [5]. Other smart materials such as piezoelectric (ferroelectric) ceramics, fluidic flexible matrix composites and electroactive polymers have been widely utilized for morphing applications [6–13].

The majority of aircrafts today use stiffened metallic (typically aluminum alloy) panels as an outer skin, although high specific strength and stiffness fiber reinforced polymer composites in the form of glass or carbon fiber/epoxies are increasingly being employed [14]. However these highlights the difficulties inherent in replacing the current stiff and strong solutions with a more flexible approach in the morphing aircraft field [14–17]. A morphing skin can be envisaged as an aerodynamic fairing to cover an underlying

Figure 1. Pneumatic muscle fibers.

morphing structure [14]. So the morphing skin is significant for realizing the morphing aircraft. Leng *et al* [17] proposed one kind of variable stiffness skin embedded with pneumatic muscle fiber (PMF). The transverse stiffness of morphing skin can be regulated by changing the internal air pressure [17]. In recent years pneumatic artificial muscle (PAM), as a kind of lightweight, low-cost and efficient actuator, has attracted worldwide attentions [18]. Wereley *et al* [19, 20] employed PAM and millimeter scale PAM for actuators of morphing structure and small unmanned aerial vehicle (UAV), respectively, due to small size characteristics millimeter scale PAM could be better applied in the small and micro UAV, miniature robot [21–24]. Larry *et al* [25], also in 2013, created a shape-changing panel with embedded McKibben-like into neat elastomer. They investigated the effect of actuator spacing and modeling methods on the performance of these panels. Nonlinear 'laminated plate' and 'rod and plate' finite element (FE) models of individual (non-embedded) RMAs and panels with embedded RMAs were developed.

In this study, one kind of active morphing skin was manufactured and was employed for camber morphing structure. Altering the camber of the adaptive airfoil was achieved by employing this kind of active morphing skin. Other than the complex and heavy structure used for variable geometry airfoils in the mission adaptive wing [26], the active morphing skin itself could be used as actuators to change the airfoil chord and camber in this study.

2. Fabrication and test of morphing skins

2.1. Fabrication of PMF and morphing skins

As to developing the fabrication process for PMFs employed in the morphing skins, the low-cost commercial materials were used to assemble the PMF and the final product interfaced easily with test setup and morphing skins. Other than the PMF proposed in the Leng *et al* [17] utilized polyvinyl chloride tube as a conduit for the injection of working fluid, the metal ending fittings were machined.

The PMFs in this study are not only high performance actuators but also the parts of the morphing skins (figure 1). The PMF utilized in this study had an average active length of 125.12 mm and a diameter of 3.50 mm. One of the ending fittings with a through hole had an outer diameter and wall inner diameter of 3.00 mm and 2.00 mm, respectively. The other ending fitting had an outer diameter of 3.00 mm. The latex tube used for the bladder had an inner diameter of 2 mm with a wall thickness of 0.5 mm. The PET braided sleeve had a nominal diameter of 3.00 mm at ±27° braid angle.

When manufacturing the morphing skins in this study, it was required that the skins could be flexible and actuated for camber morphing structures. Furthermore, the designed morphing skin itself could be used as actuators to change the airfoil chord and camber. So the silicone rubber (BJB TC5005 A-B/C) and PMFs were chosen as the basic materials to manufacture the skins. Prior to fabrication of morphing skins, the six PMFs with approximate same size were prepared, as seen in table 1. The morphing skin specimen (150 mm × 50 mm × 6.6 mm) was obtained, as shown in figure 2.

2.2. Experimental procedure of PMFs and morphing skins

As is seen in figure 3, the PMFs and morphing skins underwent quasi-static testing using a 500 N Zwick servo-hydraulic test machine (Zwick Company, Germany) to characterize the performance of PMF and morphing skins. This machine could provide the force measurements; meanwhile the displacement could be regulated smoothly during the testing. An air compressor could provide air supply for PMFs. And the pressure transducer (SMC Company, Japan), pressure governor (Hongqi instrument Company, China) were used to monitor the air pressure supplied to the PMFs accurately.

The overall goal of the experimental characterization was to determine the evolution of force with displacement for a range of internal pressures. This was achieved by first inflating the PMF to a specific pressure, ranging from 0.15 to 0.35 MPa in 0.05 MPa increments, with both ends fixed by the Zwick grips. After holding for a while under this condition, the value of maximum output force of PMF could be noted at each specific pressure. Meanwhile the value of minimum output force of PMF was zero if allowed the PMF to fully contract to the maximum contraction at each specific pressure. Finally, the PMF was compressed back to its full contraction length and then was stretched back to its nominal resting length. A given test of the PMF consisted of these cycles. This test procedure provided data to characterize the entire PMF load line, and two main points of interest obtained from this test were the blocked force and free contraction of the PMF. The blocked force is the maximum amount of force that the PMF is able to exert at a given internal pressure. Conversely, free contraction denoted the maximum stroke of the PMF for a given pressure, which was measured as the amount of contraction at which the PMF no longer provides any force.

The performance of morphing skins was tested with the same test machine and methods such as the above experimental characterization of PMF. In the figure 4, the six PMFs at pre-stretching length state (0 MPa) and in the free contraction state (0.35 MPa) were described.

2.3. The test results of PMFs and morphing skins

2.3.1. The test results of PMFs. The results of performance test of a single PMF are shown in figure 5 to demonstrate the

Table 1. The active length and outer diameter of six PMFs.

	PMF I	PMF II	PMF III	PMF IV	PMF V	PMF VI
Active length (mm)	125.04	125.04	125.03	124.56	125.86	125.16
Outer diameter (mm)	3.5	3.5	3.5	3.5	3.5	3.5

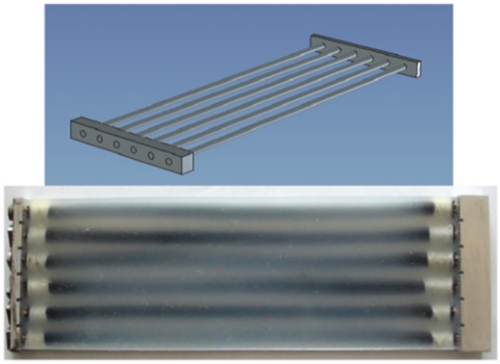

Figure 2. A bio-inspired, active morphing skins.

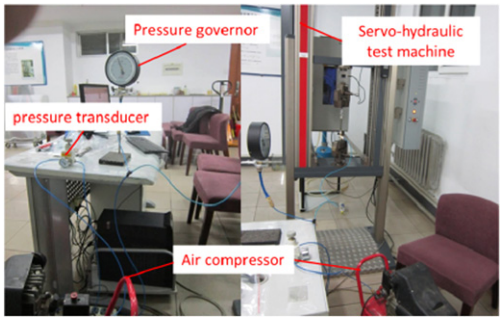

Figure 3. The experimental setup related to the test of pneumatic muscle fiber.

Figure 4. Depiction of six PMFs in the resting length (0 MPa) and in the free contraction state (0.35 MPa).

output force versus contraction ratio at a series of discrete internal pressures. The contraction ratio of PMF could be given by

$$\lambda = \frac{L_0 - l}{L_0}, \tag{1}$$

where the active length of PMF is L_0 and l is the length of PMF which has contracted.

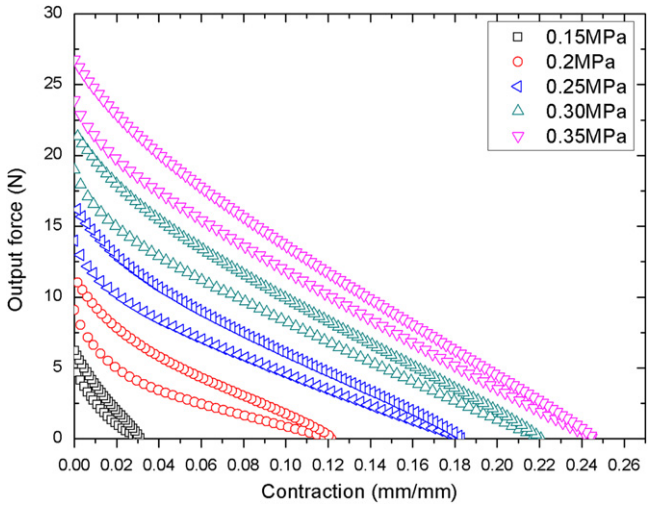

Figure 5. Six sets of test data for (a) free contraction and (b) blocked force of PMFs.

As is seen in figure 5, output force lines of PMF have obvious hysteresis, with the lower line corresponding to the path from output force to free contraction and the upper line corresponding to the return path. This results from friction between the braid and bladder during inflation and deflation, as well as friction between the individual fibers of the braid as the braid angle changes [18]. Also, damping in the elastomeric bladder may contribute to this effect [27, 28].

The PMF output force lines in figure 5 clearly show that the output force of PMF decreases with increasing contraction at a given pressure. It can be also seen that the behavior of the curve changes depending on the amount of contraction is undergoing. Below about contraction = 0.04, the force drops relatively quickly with increasing contraction. When the PMF contracts above contraction = 0.04, however, the force decreases at a slower rate along a nearly linear path. This inflection in the curve is most likely attributable to the nature of the millimeter-scale latex bladder.

As is mentioned above, two main parameters of interest are the blocked force and free contraction of the PMF at each internal pressure. These values are represented in figure 5 as the points at which the PMF output force lines reach each axis (blocked force on the vertical axis and free contraction on the horizontal axis). Obviously in figure 5 both blocked force and free contraction increase with the increase of pressure.

In order to manufacture the morphing skins, at least six PMFs should be fabricated in this study (in figure 2). More than six PMFs were fabricated. Through the testing performance of these PMFs, six PMFs with the most consistent performance were finally chosen to manufacture the morphing skins.

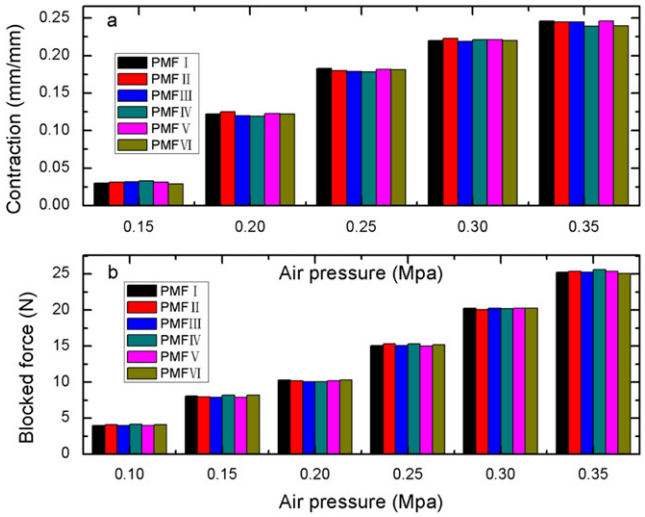

Figure 6. Experimentally characterized output force curves of PMF at a series of discrete actuation pressures.

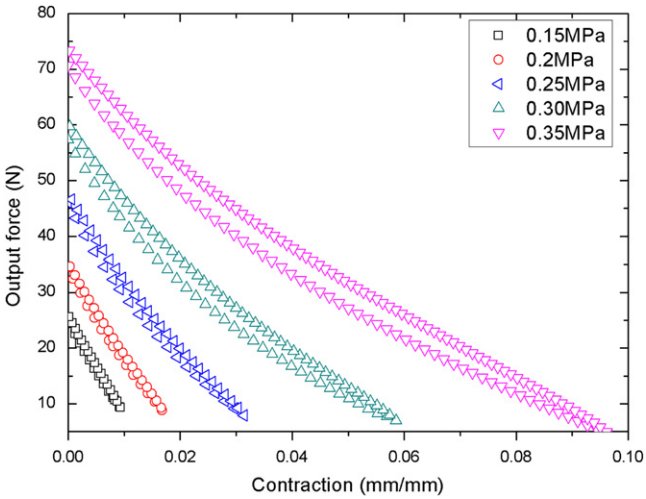

Figure 7. Experimentally characterized output force curves of morphing skins at a series of discrete actuation pressures.

As is seen in figure 6(b), the blocked forces exerted by six PMFs are in close proximity to the same value. On the other hand, the free contractions of six PMFs (in figure 6(a)) also show the same characteristics. The uniformity between PMFs could be guaranteed by employing these six chosen PMFs for manufacturing the morphing skins.

2.3.2. The test results of morphing skins. The results of performance test of morphing skins are shown in figure 7 to demonstrate the output force versus contraction ratio at a series of discrete internal pressures. It is revealed that the output force of morphing skins decreases with contraction increasing at a given pressure and both blocked force and free contraction increasing with the increase of pressure.

It is also revealed that the behavior of the morphing skins curve is different from a single PMF curve. Output force lines of morphing skins have obvious nonlinearity. This nonlinearity is most likely attributable to the nonlinearity of the

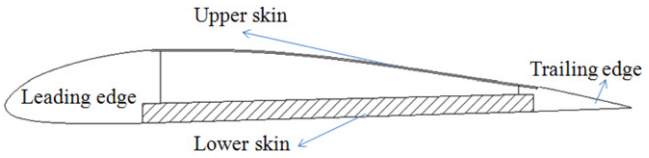

Figure 8. Substructure of the variable camber wing panel.

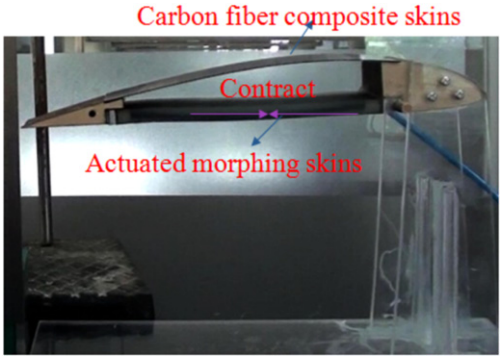

Figure 9. The variable camber wing panel.

elastomer employed to manufacture morphing skins. While supplying the work fluid into the six PMFs which are parts of the morphing skins, the length of each PMF decreases at the free contraction state and the silicone rubber, as the matrix of the morphing skins, would also contract passively. Therefore the output force curves of this morphing skin have obvious nonlinearity.

3. Structural design of the camber morphing structure

The morphing concept of a variable camber wing is shown in figure 8. The wing panel was manufactured with the airfoil of CLARK Y, the chord being 250 mm, and the span direction length being 50 mm which matches with the size of morphing skins. The carbon fiber composite plate was used as the upper surface skin of the wing panel and the manufactured active morphing skins were utilized as the lower surface skin of the wing panel. As is seen in figure 9, the variable camber wing panel with the active morphing skins was manufactured.

In the conventional aircraft control surfaces and the proposed structural concept, aileron assembled on the wing tip of the trailing edge is a small piece of movable wing surface. A deflection of the aileron creates the aerodynamic force to realize the maneuver of the aircraft. However morphing aircrafts are capable of altering their shape to meet changing mission requirements of the aircrafts and to perform flight control without the use of conventional control surfaces. An alternative approach to modifying the aerodynamic characteristics of a wing is to alter the wing out of its original plane. In this study the developed variable geometry airfoils abandoned the complex and heavy structure. An adaptive airfoil that relies on the previous active morphing skin achieved reversing shape change. Due to the morphing skin actuating the skin itself and the adaptive airfoil, the extra

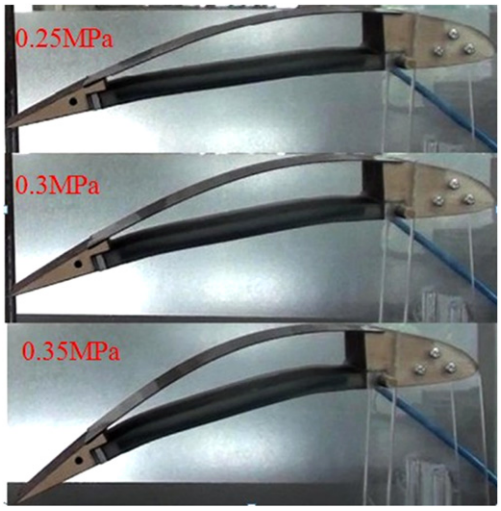

Figure 10. The active morphing skin actuate the variable camber wing at different actuation pressures.

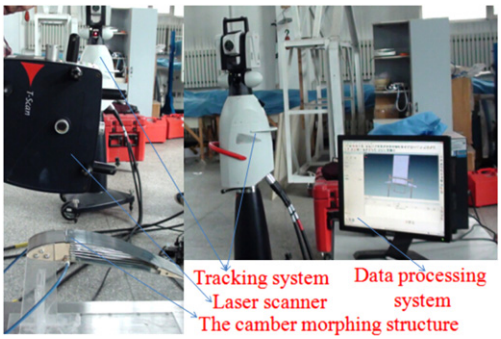

Figure 11. The deformation experimental setup related to the test of the camber morphing structure.

actuators are no longer needed to reduce the weight of the structure.

Figure 10 shows a side view of the variable camber wing actuated by the active morphing skins at different actuation pressures. The carbon fiber composite skin is 0.6 mm thick and was attached on the upper surface of the wing panel. The active morphing skin was attached on the lower surface of the wing panel (as seen in figures 9 and 10). Obviously the wing cambered more greatly while the actuation pressure increased. Meanwhile the whole shape change process is reversible and the wing could camber quickly due to the morphing skin actuated by the compressed air.

4. Experiment and finite element method (FEM) analysis of the camber morphing structures

4.1. Deformation measurement of the camber morphing structures

As is seen in figure 11, the variable camber wing panel with the active morphing skins underwent three-dimensional laser scanning utilizing a T-scan handheld scanner (T-scan Company, Switzerland) to characterize the camber and airfoil of

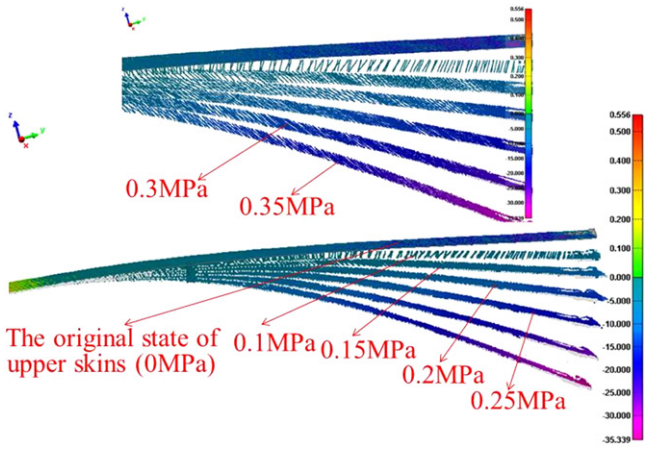

Figure 12. The three-dimensional coordinates' cloud of the upper skins at different actuated air pressures.

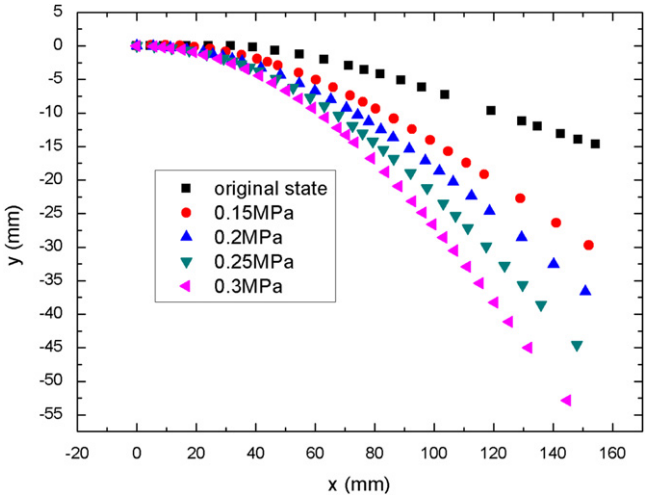

Figure 13. Comparison between original shape of the airfoil (morphing skins were actuated at 0 MPa) and deformed shapes of the airfoil (morphing skins were actuated at a series of discrete actuator pressures varying from 0.1 to 0.3 MPa).

the camber morphing structures. The three-dimensional coordinates of the wing panel upper skins were measured though this three-dimensional laser scanning system. The three-dimensional coordinates' cloud of the wing panel upper skins at different actuated air pressures could be seen in figure 12.

From figure 13 the original shape of the upper surface skins (morphing skins were actuated at 0 MPa) and deformed shapes of the upper surface skins (morphing skins were actuated at a series of discrete actuator pressures varying from 0.15 to 0.3 MPa) could be seen through analyzing the three-dimensional coordinates of the upper skins at different actuated air pressures.

4.2. FEM analysis of the camber morphing structures

4.2.1. Design of FE model. The FE model is the same as the actual manufacturing structures. The model included three parts: leading edge, upper surface skins and trailing edge. The

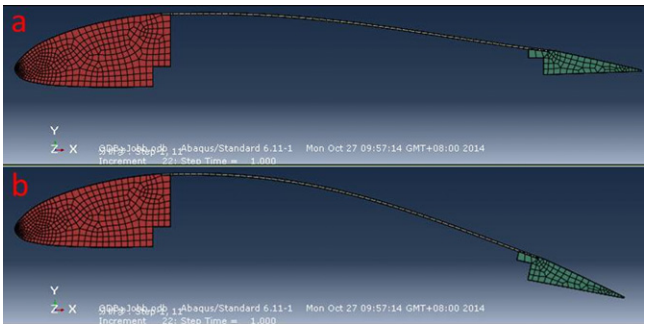

Figure 14. The camber morphing structures model of FEM analysis. (a) The original shape of the camber morphing structures model. (b) The deformed shape of the camber morphing structures model (morphing skins were actuated at 0.15 MPa).

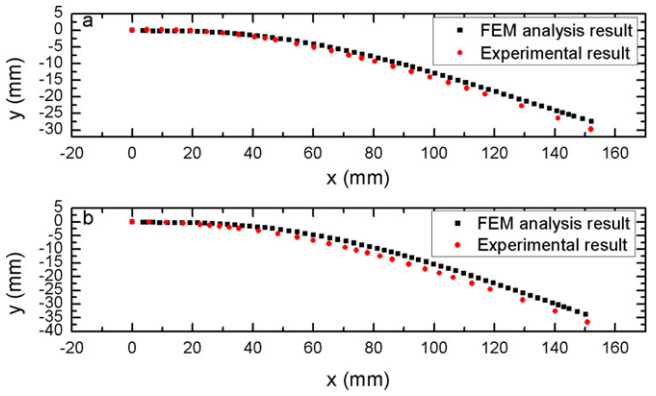

Figure 15. Comparison between experimental result and FEM analysis result of deformed shape of the upper surface skins. (a) Morphing skins were actuated at 0.15 MPa. (b) Morphing skins were actuated at 0.2 MPa.

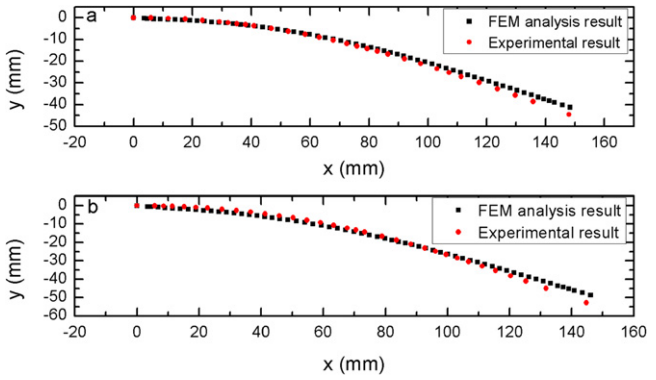

Figure 16. Comparison between experimental result and FEM analysis result of deformed shape of the upper surface skins. (a) Morphing skins were actuated at 0.25 MPa. (b) Morphing skins were actuated at 0.3 MPa.

boundary condition was set as fixed end on leading edge and upper skins were tied with leading edge and trailing edge.

As is mentioned above, the carbon fiber composite plate with 0.6 mm thickness was used as the upper surface skins. The carbon fiber composite plate is commercial orthotropic plate (Wasse Company, China). The mechanical properties of this orthotropic plate are in accord with the technical parameters manufacturers provided through tensile testing of the orthotropic plate. FE material property settings of upper surface skins are shown below: elastic modulus of x axis being 12.25 GPa, elastic modulus of y axis 12.25 GPa, shear modulus 0.073 GPa, and Poisson ratio 0.27. Compared with upper surface skins, the stiffness of the leading edge and trailing edge is big enough, so in the analysis process the leading edge and trailing edge are considered to be rigid. The model after meshing is shown in figure 14(a).

Through the laser scan deformation measurement of the camber morphing structures, the contraction of the active morphing skins could be calculated. Then the output force of the active morphing skins could be obtained from figure 7 as the camber morphing structures deformed at different actuator pressures. As seen in table 2, output force and contraction of the active morphing skin were obtained in the camber morphing process at different actuator pressures. In the FE model the leading edge was completely fixed and the actuated force was applied to connection area between the active morphing skin and the trailing edge. The option that the direction of the actuated force followed the structure deformation was selected in the FE model.

After the following procedures: opening the material function database of ABAQUS, selecting various parameters and applying loads, choosing geometrical large deformation option, running the calculation, the result of upper surface skins displacement map is expressed as follows.

4.2.2. FEM calculation deformation of the upper surface skins in the camber morphing structures. According to FEM analysis results, the deformed shape of the camber morphing structures model is shown in figure 14(b). With the camber morphing structures deforming, the nodes of the upper surface skins were extracted. From figures 15 and 16 experimental result and FEM analysis result of deformed shapes of the upper surface skins were compared (morphing skins were actuated at a series of discrete actuator pressures varying from 0.15 to 0.3 MPa). It is clearly seen that FEM analysis result is in close proximity to experimental result.

Table 2. Output force active morphing skin provided in the camber morphing process.

	0.15 MPa	0.2 MPa	0.25 MPa	0.25 MPa
Contraction	0.00816	0.01096	0.01808	0.02432
Output force (N)	10.79	16.08	19.9	27.97

5. Conclusions

A bio-inspire active morphing skin was manufactured and was utilized for camber morphing structures. A kind of PMF used for fabricating morphing skin was manufactured. This PMF could output force reaching 26.77 N and contract 0.246 (24.6%) only at 0.35 MPa, meanwhile this PMF could be more easily employed in the morphing structure compared with other PAMs and PMFs because of its millimeter-scale

with a nominal diameter of 3.50 mm. The active morphing skin which employed six PMFs could output force 73.59 N and contract 0.097 (9.7%) only at 0.35 MPa. An adaptive airfoil that relies on the active morphing skin achieved reversing shape change. The deformed shapes of this chordwise bending airfoil structure were obtained when the morphing skin was actuated at a series of discrete actuator pressures varying from 0.1 to 0.3 MPa. Meanwhile this chordwise bending airfoil structure was analyzed through FEM. The deformed shapes of the upper surface skin could be obtained from FEM analysis results. Furthermore the morphing skin itself could be used as actuators to change the airfoil chord and camber without other additional actuators.

Research in this active morphing skin is still in the preliminary stage. Each category of mechanism concluding skin manufacture technology, skin actuation properties and aerostructural properties of morphing airfoil should be studied independently, with the goal of integrating these components into a complete system. Ultimately, a full understanding of the performance of this active morphing skin and morphing airfoil would make it possible that the future morphing aircraft utilized this bio-inspire active morphing skin could fly like a bird.

Acknowledgments

The author wishes to thank the late Professor Ephrahim Garcia who provided very helpful advice for this study.

References

[1] Manzo J, Garcia E, Wickenheiser A and Horner G C 2004 Adaptive structural systems and compliant skin technology of morphing aircraft structures *Proc. SPIE* **5390** 225–34
[2] Anderson J D 1985 *Introduction to Flight* 2nd edn (New York: McGraw-Hill)
[3] Barbarino S, Bilgen O, Ajaj R M, Friswell M I and Inman D J 2011 A review of morphing aircraft *J. Intell. Mater. Syst. Struct.* **22** 823–77
[4] Sofla A Y N, Meguid A S, Tan K T and Yeo W K 2010 Shape morphing of aircraft wing: status and challenges *Mater. Des.* **31** 1284–392
[5] Elzey D M, Sofla A Y N and Wadley H N G 2003 A bio-inspired, high-authority actuator for shape morphing structures *Proc. SPIE* **5053** 92–100
[6] Straub F K, Ngo H T, Anand V and Domzalski D B 2001 Development of a piezoelectric actuator for trailing edge flap control of full scale rotor blades *Smart Mater. Struct.* **10** 25–34
[7] Lee T and Chopra I 2001 Design of piezostack-driven trailing-edge flap actuators for helicopter rotors *Smart Mater. Struct.* **10** 15–24
[8] Kim J S, Wang K W and Smith E C 2001 High-authority piezoelectric actuation system synthesis through mechanical resonance and electrical tailoring *J. Intell. Mater. Syst. Struct.* **16** 21–31
[9] Chopra I 2002 Review of state of art of smart structures and integrated systems *AIAA J.* **40** 2145–87
[10] Philen M, Shan Y, Bakis C E, Wang K W and Rahn D 2006 Variable stiffness adaptive structures utilizing hydraulically pressurized flexible matrix composites with valve control *47th AIAA/ASME/ASCE/AHS/ASC Structures, Structural Dynamics and Materials Conf. (Newport, RI)*
[11] Philen M, Phillips D and Baur J 2009 Variable modulus materials based upon F2MC reinforced shape memory polymers *50th AIAA/ASME/ASCE/AHS/ASC Structures, Structural Dynamics and Materials Conf. (Palm Springs, CA)*
[12] Shan Y, Philen M, Lotfi A, Li S, Bakis C E, Rahn C D and Wang K W 2009 Variable stiffness structures utilizing fluidic flexible matrix composites *J. Intell. Mater. Syst. Struct.* **20** 443–56
[13] Chou A and Philen M 2008 High performance flexible matrix composite actuators for trailing edge flap control *Virginia Space Grant Consortium Student Research Conf. (Norfolk, Virginia)*
[14] Thill C, Etches J, Bond I, Potter K and Weaver P 2008 Morphing skins *Aeronaut. J.* **112** 117–39
[15] Sanders B, Joo J J and Reich G W 2006 Conceptual skin design for morphing aircraft *16th Int. Conf. on Adaptive Structures and Technologies*
[16] Sanders B, Eastep F E and Forster E 2003 Aerodynamic and aeroelastic characteristics of wings with conformal control surfaces for morphing aircraft *J. Aircr.* **40** 94–9
[17] Chen Y, Yin W, Liu Y and Leng J 2011 Structural design and analysis of morphing skin embedded with pneumatic muscle fibers *Smart Mater. Struct.* **20** 085033
[18] Daerden F and Lefeber D 2002 Pneumatic artificial muscles: actuators for robotics and automation *Eur. J. Mechan. Environ. Eng.* **47** 11–21
[19] Wereley N M, Kothera C, Bubert E, Woods B, Gentry M and Vocke R 2009 Pneumatic artificial muscles for aerospace applications *50th AIAA/ASME/ASCE/AHS/ASC Structures and Structural Dynamics and Materials Conf.* 82584 2009–2140
[20] Woods B K S, Friswell M I and Wereley N M 2014 Advanced kinematic tailoring for morphing aircraft actuation *AIAA J.* **52** 788–98
[21] Hocking E G and Wereley N M 2012 Fabrication and characterization of fluidic artificial muscles having millimeter-scale diameters *Proc. SPIE* **8341** 83410
[22] Ozkan M, Inoue K, Negishi K and Yamanaka T 2000 Defining a neural network controller structure for a rubbertuator robot *Neural Netw.* **13** 533–44
[23] Tondu B, Ippolito S and Guiochet J 2005 A seven-degrees-of-freedom robot-arm driven by pneumatic artificial muscles for humanoid robots *Int. J. Robot. Res.* **24** 257–74
[24] Ferris D, Czerniecki J M and Hannaford B 2005 An ankle-foot orthosis powered by artificial pneumatic muscles *J. Appl. Biomech.* **21** 189–97
[25] Powers S G, Webb L D, Firend E L and Kolos W A 1992 Flight test results from a supercritical mission adaptive wing with smooth variable camber *The AIAA 6th Biennial Conf.*
[26] Peel L D, Molina E Jr, Baur J W and Justice R S 2013 Characterization and application of shape-changing panels with embedded rubber muscle actuators *Smart Mater. Struct.* **22** 094020
[27] Chou C and Hannaford B 1994 Static and dynamic characteristics of McKibben pneumatic artificial muscles *Proc. ICRA* **1** 281–6
[28] Kothera C, Jangid M, Sirohi J and Wereley N M 2009 Experimental characterization and static modeling of McKibben actuators *ASME Int. Mech. Eng. Congr. Exposition* **131** 091010